Solar Energy Materials & Solar Cells 163 (2017) 250–254

Contents lists available at ScienceDirect

Solar Energy Materials & Solar Cells

journal homepage: www.elsevier.com/locate/solmat

$CH_3NH_3PbI_3$ converted from reactive magnetron sputtered PbO for large area perovskite solar cells

Zhirong Zhang[a,b], Meicheng Li[a,*], Wenjian Liu[a], Xiaopeng Yue[a,c], Peng Cui[a], Dong Wei[a]

[a] State Key Laboratory of Alternate Electrical Power System with Renewable Energy Sources, North China Electric Power University, Beijing 102206, China
[b] Institute of New Energy, HeXi University, Zhangye, Gansu 734000, China
[c] Key Laboratory of Resource Exploration Research of Hebei Province, Hebei University of Engineering, Handan, Hebei 056038, China

ARTICLE INFO

Keywords:
Reactive magnetron sputtered
Large area
Perovskite
Solar cells

ABSTRACT

Adopting DC reactive magnetron sputtering technique, PbO film was fabricated on FTO-glass substrate coated with a nanocrystalline rutile titania (NRT) by using a pure metallic lead target in an Ar/O_2 mixture. Then the as-prepared PbO film was converted to $CH_3NH_3PbI_3$ through the sequential reactions occurred in isopropanol solution of CH_3NH_3I. The as-prepared perovskite film exhibits a surface morphology of high uniformity and good coverage over a large scale; the crystal grains reach the size of up to 600 nm, which is beneficial for enhancing light absorption and decreasing grain boundary. The solar cells with a structure of FTO/NRT/$CH_3NH_3PbI_3$/Spiro-MeOTAD/Au were fabricated, where NRT was employed as the contact layer of the photovoltaic devices. Our champion cells with active area of 0.09 cm^2 and 1.07 cm^2 achieve the highest power conversion efficiency of 14.1% and 10.7%, respectively, under the standard AM 1.5 conditions. The present approach is competent for the fabrication of large area perovskite solar cells with the advantages of easy control, cost-saving, and less use of toxic reagents, and thus with potential applications.

1. Introduction

In recent years, there is an ever-increasing attention to organic–inorganic metal halide perovskites materials, whose classic representatives include $CH_3NH_3PbI_3$, $CH_3NH_3PbI_{3-x}Cl_x$ and $CH(NH_2)_2PbI_3$. These materials exhibit many impressively unique properties, such as strong absorption coefficients, long exciton diffusion length, ease of synthesis, low cost and environmental-friendliness [1–4]. Thanks to such advantages, perovskite solar cells (PSCs) have made great progresses, exhibiting a surging power conversion efficiency (PCE)—from around 10% in mid-2012 to more than 20% at present [5,6], and further improvements are expected. Meanwhile, the various studies on its performance optimizations as well as process ameliorations have been proceeding, and some significant technological or scientific progresses are obtained [7–10], which are more important than a high PCE for its further development in some sense.

The quality and morphology of the perovskite films are crucial to its photoelectric properties, and then directly affect the performance of the resultant PSCs. Although the several deposition methods have been proposed to fabricate the perovskite light-absorption layers [11–13], it is still a great challenge to the fabrication of perovskite films with satisfactory coverage and uniformity over a large area. For instance, the so-called one step precursor deposition and sequential deposition process are used most widely owing to their distinct advantages (solution-processable, easy to operate, low-cost, *etc.*), and the PSCs with high PCE nearly 20% can be obtained by any of the two process routes [6,14]. However, these methods are applicable only to fabrication of the devices with a small active area (around 0.1 cm^2 or smaller). This is mainly because the magnitude of centrifugal force generated by planar rotation changes along the radial direction of the substrates intrinsically, and such changes tend to be more striking with the increase of spinning area. So it is hard to obtain a film with adequate uniformity by using spin-coating process. While as for those tiny cells, they are always criticized due to the larger measurement errors on the one hand and impractical size for applications on the other. Liu et al. proposed a dual-source vapor deposition technique to prepare a mixed halide perovskite $CH_3NH_3PbI_{3-x}Cl_x$ layer [12], which is spin-coating-free, thus exhibiting the potential to form the large area perovskite films with high coverage and uniformity. However, this approach requires the vacuum environment and high temperature, which would increase the cost of large-scale fabrication significantly; coupled with its intractable controllability, it seems to be not a preferred route for manufacture. Perhaps, partly due to the predicament of the fabrication process, there are only fewer literatures on PSCs with an active area at

* Corresponding author.
E-mail address: mcli@ncepu.edu.cn (M. Li).

http://dx.doi.org/10.1016/j.solmat.2017.01.034
Received 7 July 2016; Received in revised form 14 January 2017; Accepted 22 January 2017

centimeter-scale up to now, and most of the reported devices (including some PSCs modules) are prepared by using spin-coating or evaporation process yet [15–21], which suffer from the limitations and disadvantages as mentioned above. Therefore, it is highly necessary to develop applicable deposition methods for the fabrication of perovskite film (or PSCs) with large area.

The study reported by Razza et al. is compelling—they used the blade coating technique to deposit PbI_2 layer as the first step of a sequential step deposition route for $CH_3NH_3PbI_3$ formation, achieving the best PCE of 10.3% for a 10.1 cm^2 module composed by a series connection of four 2.5 cm^2 cells [22]. Besides, Song et al. reported that $CH_3NH_3PbI_3$ can be obtained starting from electrodepositing PbO, and then reaction with CH_3NH_3I [23,24]. These two approaches both have the potential advantages to apply to industrial production.

Motivated by the same expectation for exploring the deposition method that is practical to fabrication the large area PSCs, here we present a novel process route based on DC reactive magnetron sputtering (DRMS) to prepare $CH_3NH_3PbI_3$ film. It is generally known that DRMS is an important industrial process for the deposition of metal–oxide films from elemental targets, which has the specific advantages for film growth, such as high packing density, good interfacial adhesion to substrate and easy control. In this article, we report a pure metallic lead target was sputtered in an oxygen–argon atmosphere to grow PbO film with high continuity and uniformity; and then the as-prepared PbO was converted to $CH_3NH_3PbI_3$ through the sequential reactions by immersing it into a solution of CH_3NH_3I in isopropanol. The resultant perovskite film exhibits considerable good uniformity and coverage over a large scale. As a result, the PSCs with a structure of a FTO/NRT/$CH_3NH_3PbI_3$/Spiro-MeOTAD/Au and an active area of 1.07 cm^2 yield a best PCE of 10.7% (the average value of PCE is 9.8 ± 0.9%) under standard AM 1.5 conditions. The present approach is spin-coating-free for the formation of large area $CH_3NH_3PbI_3$ film with the advantages of easy control, cost-saving, and less use of toxic reagents; what's more, it is expected to be used for the manufacture of PSCs or other thin-film devices.

2. Material and methods

2.1. Materials

Unless stated otherwise, all materials were purchased from Sigma-Aldrich or Acros Organics and used as received. Spiro-MeOTAD was purchased from Merck KGaA. FTO glasses of 2.2 mm thickness and less than 20 Ω sq^{-1}. were purchased from Pilkington. CH_3NH_3I was prepared as reported elsewhere [5].

2.2. Fabrication of solar cells

Devices were fabricated on fluorine-doped tin oxide (FTO) coated glass with a sheet resistances of 20 Ω sq^{-1}. Initially FTO was removed from regions under the anode contact, to prevent shunting upon contact with measurement pins, by etching the FTO with HCl and zinc powder. The substrates were then cleaned sequentially in soap (2% Hellmanex in water), acetone, ethanol, deionized water and finally treated under oxygen plasma to remove the last traces of organic residues. To deposit the nanocrystalline of rutile titania (NRT), they were immersed in 200 mM aqueous solution of titanium tetrachloride ($TiCl_4$) in a closed vessel and kept in a water bath at 70 °C for 1 h, then rinsed with deionized water and ethanol. Lead oxide films were prepared on NRT-coated substrates by DC reactive magnetron sputtering of a metallic lead target (with a diameter of 58 mm) in an Ar–O_2 mixture. In this study, Ar/O_2 ratio is maintained at 22:10, where the oxygen partial pressure is controlled by regulating the oxygen flow rate. Initially the chamber pressure was pumped down until the vacuum reached 10^{-7} Torr. For sample preparation, the pressure was maintained at 5.5×10^{-3} Torr, with a constant discharge current of 100 mA (≈32 W). To prepare the perovskite layers, the samples were dipped into CH_3NH_3I solution dissolved in 2-propanol (40 mg mL^{-1}) for 10 min and then annealed at 100 °C for 30 min. A hole-transporting layer (HTL) was then deposited via spin-coating a 0.79 M solution of spiroMeOTAD in chlorobenzene, with additives of lithium bis(trifluoromethanesulfonyl) imide and 4-*tert*-butylpyridine. Devices were then left overnight in air for the spiroOMeTAD to dope via oxidation. Finally, the gold electrodes were deposited on top of the HTL layer through a metal shadow mask via magnetron sputtering with a low current intensity of 5 mA, to finish the fabrication.

2.3. Measurement methods

X-ray diffraction (XRD) spectra were measured with a Panalytical X'Pert Pro x-ray diffractometer using Cu Kα radiation at 40 kV and 40 mA. A field emission scanning electron microscope (SEM, HITACHI UHR FE-SEM SU8200) was used to acquire SEM images. The optical absorption of perovskite films were studied by Shimadzu Ultraviolet-Visible (UV–vis) spectrophotometer (UV 2600). The current density-voltage (*J-V*) curves were measured using a digital source meter (Keithley Model 2400) to apply an external potential bias to the solar cells and measuring the generated photocurrent. The emission spectrum from a xenon lamp (Oriel, 450 W) was matched to the standard AM 1.5G. The exact light intensities of the measurements were determined using a calibrated Si diode as reference. The EQE spectra were acquired by an IPCE setup consisting of a xenon lamp (Oriel, 450 W) as the light source, a monochromator, a chopper with a frequency of 100 Hz, a lock-in amplifier, and a Si diode for calibration.

3. Results and discussion

The fabrication processes for $CH_3NH_3PbI_3$ film converted from reactive magnetron sputtered PbO are schematically illustrated in Fig. 1, and the experimental details are described as mentioned above.

Prior to the sputtering, a NRT layer was deposited on FTO substrate by a chemical bath deposition method, which severs as a contact layer of the PSCs [25]. As the top-view of scanning electron microscope (SEM) in Fig. 2(a) shows, the as-prepared NRT film exhibits a loosen-structured morphology; its high uniformity over large-scale attributes to the homogeneous liquid phase environment in which the film have grown. To form PbO film, a metallic lead target (58 mm diameter) was used and sputtered in an oxygen–argon mixture, where the oxygen partial pressure is controlled by regulating the oxygen flow rate. The distance between the target and the substrate sample is 70 mm. After

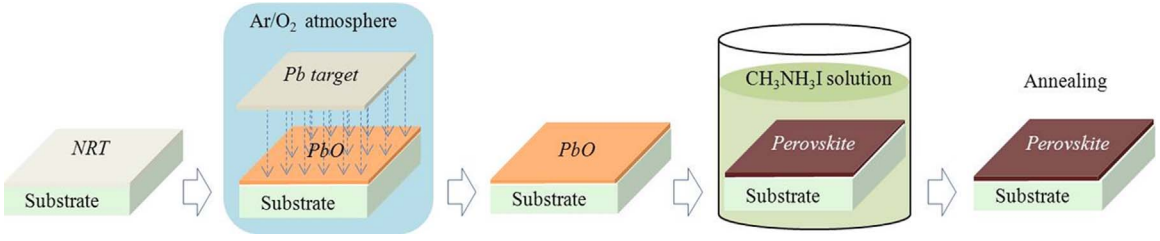

Fig. 1. Schematic illustration of $CH_3NH_3PbI_3$ formation (on NRT-coated FTO glass substrate) through the sputtered PbO.

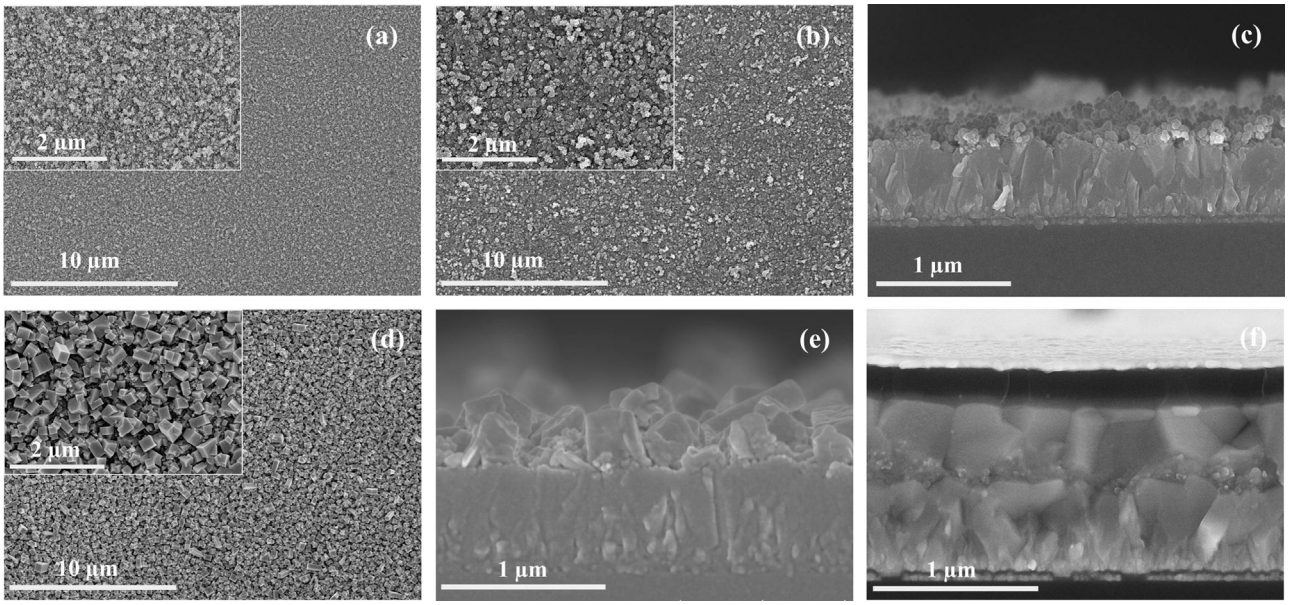

Fig. 2. Thin-film topology characterization. (a), (b) and (d) are the top- view SEM of NRT, sputtered PbO, $CH_3NH_3PbI_3$, respectively, where the insertions are the corresponding one with high magnification. (c), (e) and (f) are the corresponding cross-sectional SEM of PbO, $CH_3NH_3PbI_3$, the whole device, respectively.

the sputtering, the substrate takes on a slight opaque red color, indicating the formation of PbO. Its top-view SEM with different magnification are presented Fig. 2(b), and the morphology similar to that of NRT can be observed, uniform and loose over a macroscopic scale. Fig. 2(c) shows the cross-sectional SEM of the resultant PbO film, evidencing that it has an average thickness of 110 nm or so, which can be conveniently tuned by sputtering time. It was reported that the expected thickness of $CH_3NH_3PbI_3$ layer converted from PbO would be 5–6 times than that of PbO film itself because of the volume expansion as a result of interdiffusion reaction [24]. In this study, given the loose morphology of PbO film resulted from the loosen-structured NRT, 3–4 times expansion of the film thickness is expected (it is confirmed by the characteristic of the resultant $CH_3NH_3PbI_3$ film as below). Additionally, the cross-sectional SEM images show the sputtered PbO permeated into NRT layer sufficiently for its loosen-structured morphology, thus leading to an intimate junction of large interfacial area with the resultant perovskite, which is much more effective in extracting photogenerated electrons [25].

Subsequently, the as-prepared PbO film sample was immersed into a solution of CH_3NH_3I in isopropanol, and the substrate turned dark brown gradually, indicating the formation of $CH_3NH_3PbI_3$ perovskite. The reaction mechanism of such conversion can be described as flows: i) CH_3NH_3I in isopropanol breaks down into CH_3NH_2 and HI (Fig. 3(a)); ii) HI reacts with PbO to form PbI_2 (Fig. 3(b)); iii) $CH_3NH_3PbI_3$ is formed through the reaction between PbI_2 and CH_3NH_3I (Fig. 3(c)). For the reactions as a whole, PbI_2 is just an intermediate and absent from the end product, which is positive because its presence would cause the degeneration of device performance [26]. Remarkably, equivalent amount of H_2O was generated during the conversion process from PbO to PbI_2 (Fig. 3(b)), which only lead to modest changes in the films that do not affect the final photovoltaic performance [27], and it is even reported that the mild moisture or a small amount H_2O has a positive effect on perovskite film formation [28,29].

(a) $CH_3NH_3I \rightarrow CH_3NH_2 + HI$

(b) $PbO + HI \rightarrow PbI_2 + H_2O$

(c) $PbI_2 + CH_3NH_3I \rightarrow CH_3NH_3PbI_3$

Fig. 3. The mechanism of $CH_3NH_3PbI_3$ formation through the reactions between PbO and CH_3NH_3I solution in isopropanol.

The top-view SEM of the resultant $CH_3NH_3PbI_3$ is presented in Fig. 2(d), and it shows that the film is composed of the crystal grains with a size of 60–500 nm, exhibiting high uniformity and good coverage over a large area. Even on a macroscopical area about a dozen of square centimeters, the uniform morphology of the perovskite film can be observed by naked eyes. Especially, our experiments revealed that the surface coverage of the film as well as the grain size composted it are very sensitive to the concentration of CH_3NH_3I solution, and it was not be fully optimized in this study. The thickness of $CH_3NH_3PbI_3$ film is evidenced by its cross-sectional SEM in Fig. 2(e), which is about 430 nm, nearly 4 times thinker than that of corresponding PbO film, and that is consistent with the value expected as above.

We subsequently investigate the structural properties of the resultant films by X-ray diffraction (XRD) measurement. As a previous study reported, DRMS lead to different kinds of lead oxides, such as PbO, $PbO_{1.44}$, Pb_2O_3, and PbO_2, under the condition of different oxygen flow rate [30]. In this study, lead oxide was obtained by sputtering a pure metallic lead target in Ar/O_2 mixture with a ratio of 22:10. Fig. 4(a) shows its XRD patterns, and those of NRT/FTO substrate are also presented for comparison. The diffraction peaks of the as-prepared lead oxide film exhibit the larger values of full width half maximum (FWHM) and does not strictly correspond to any cataloged phase from JCPDS International diffraction data base, but the patterns are also a little sharp and very close to those of orthorhombic PbO (JCPDS card No. 38–1477) except a slight position shift. It is presumably caused by a mixed structure of amorphous and crystal phase of PbO, or the presence of other sub-oxides of Pb [30,31]. To form the perovskite, PbO film sample was immersed into a CH_3NH_3I solution in isopropanol to induce the chemical reactions. Then XRD patterns of the product were recorded (see Fig. 4(a)), which is in good agreement with the results in published paper [13], confirming its typical structure of $CH_3NH_3PbI_3$. Besides, no diffraction peaks of the residual PbO were detected in the patterns of the resultant perovskite, and those of PbI_2 were also absent, which indicate the conversions described in Fig. 3 are complete. These results preliminarily show that our approach is feasible and available to fabricate $CH_3NH_3PbI_3$ film. As a side note, the peaks of NRT were not detected by the typical XRD measurement, which probably resulted from its ultrathin thickness, or being concealed by the sharp peaks of others.

In addition, PbO and the resultant $CH_3NH_3PbI_3$ film were characterized by UV–vis spectroscopy as shown in Fig. 4(b). The absorption

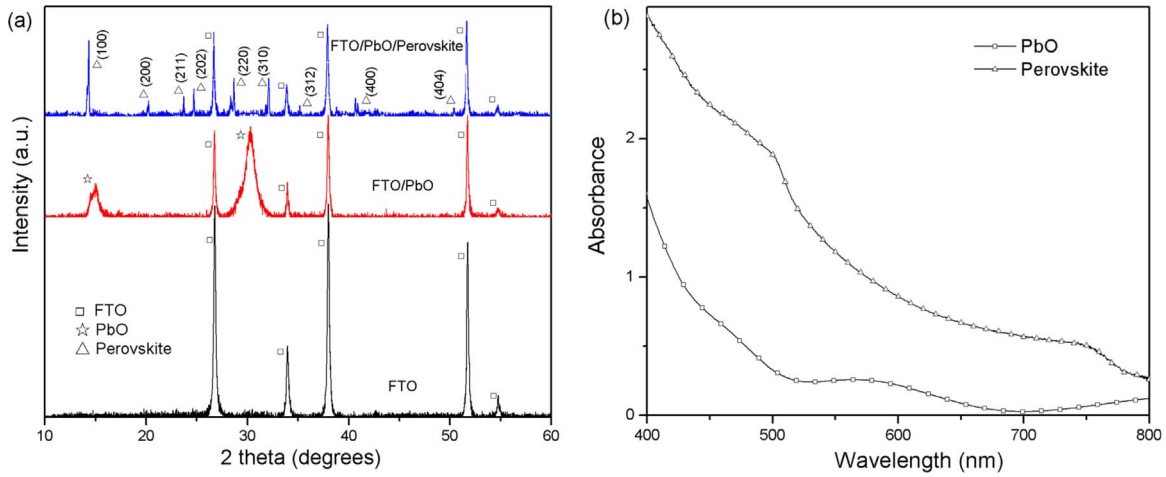

Fig. 4. (a) The XRD patterns of FTO glass coated with NRT, PbO, and $CH_3NH_3PbI_3$. (b) UV–vis spectra of PbO and $CH_3NH_3PbI_3$.

spectrum of the sputtered PbO on NRT film is in the visible short-wavelength region with the absorption onsets at ~520 and ~670 nm, respectively, similar to that of the previous report [23]. The perovskite films exhibit the typical absorption peak ~760 nm, corresponding to the direct band gap transition from the first valence band to conduction band [6], while 480 nm absorption peak corresponds to the transition from the second valence band to conduction band [3].

Using DRMS-based deposition method for formation of $CH_3NH_3PbI_3$ film, we prepared the PSCs with a structure of FTO/NRT/$CH_3NH_3PbI_3$/Spiro-MeOTAD/Au. The details of device fabrication and characterization are described as mentioned above. The as-prepared devices involve two models with different size of active area for comparison, and they are denoted as Device A (with an active area of 0.09 cm^2) and B (with an active area of 1.07 cm^2), respectively. The average PCE of Device A is 13.2% (for 12 devices), and the champion one of them yields a PCE of 14.1% with an open-circuit voltage (V_{oc}) of 1.04 V, a short-circuit current-density (J_{sc}) of 20.2 mA/cm^2, and a fill factor (FF) of 66.9%, whose current density–voltage (J–V) characteristics is presented in Fig. 5(a). All the three photovoltaic parameters (V_{oc}, J_{sc}, and FF) are comparable to the one's reported in literature 26 (the devices in this study are identical to it in construction but different in process of $CH_3NH_3PbI_3$ formation), so the feasibility and reliability of our method are confirmed. Based on the identical process, Device B were fabricated, which have an active area that is about 12 times larger than that of Device A, exhibiting an average PCE of 9.8% (for 12 devices). The top cell among them achieves an inferior PCE of 10.7%, with a V_{oc} of 1.03 V, a J_{sc} of 17.2 mA/cm^2, and a FF of 60.6%, respectively (see Fig. 5(a)). We implemented the external quantum efficiency (EQE) measurement for a representative cell among Device A and Device B, respectively. Fig. 5(b) shows EQE spectra of the two devices, which exhibit a similar spectral sensitivity in the range from the visible to the near-IR region (400–800 nm) except for the lower EQE of Device B. The integrated current densities (19.67 and 16.81 mA/cm^2 for Device A and Device B, respectively) from the EQE curve show less than *ca.* 3% mismatch compared to the J_{sc} (20.2 and 17.3 mA/cm^2) obtained from the J–V curve, where a slight mismatch of them is a general phenomenon in solar cells due to various kinds of uncertain factors.

Compared to the small-scaled Device A, Device B exhibits a decline in values of all the three photovoltaic parameters. With the increase of the device area from 0.09 cm^2 to 1.07 cm^2, the declining percentage of V_{oc}, J_{sc}, and FF is 1.0%, 14.9%, and 9.4%, respectively (for the highest performance), thus leading to a reduction of 24.1% in PCE. It clearly shows that, J_{sc} has the most significant drop; FF comes second; V_{oc} drops the most slightly. In essence, these declinations are ascribed to the higher series resistance R_s of the large-scaled Device B, which increases monotonically with larger active cell area [21], thus leading to the declination of J_{sc} and the corresponding fall of FF. As for the tiny variations of V_{oc}, it is reasonable because V_{oc} is affected very slightly as R_s changes. Therefore, to improve the photovoltaic performance of large-scale PSCs, one of the important measures is to reduce R_s by some ways. In fact, the devices reported in this paper were not optimized adequately, and the further efficiency enhancement could be expected following the optimization of the process conditions,

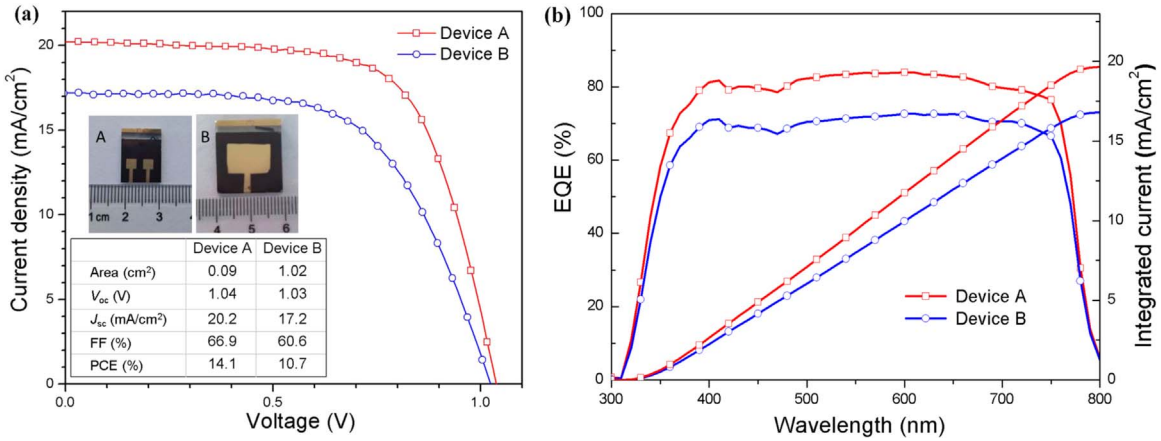

Fig. 5. (a) J-V characteristics, measured under AM 1.5 G (100 mW/cm^2), for Device A and B. The insertions are their actual photos. (b) EQE spectra of the representative devices and the corresponding integrated J_{sc}.

adjustment of parameters, morphology and relative interface modification. Finally, it should be noted that our cells also suffer from a bit hysteresis when they were measured (presented in Fig. S1 in Supplementary material). Although the origin of hysteresis is still open to debate, it could be overcome through careful surface engineering of existing TiO_2 or through a judicious choice of alternative interfacial layers [32].

4. Conclusions

In summary, a novel deposition method for formation of $CH_3NH_3PbI_3$ film was proposed, in which lead oxide was sputtered on the substrate by using DRMS, and then it was converted to the perovskite through the sequential reactions occurred in isopropanol solution of CH_3NH_3I. The results reveal that the as-prepared lead oxide film is tetragonal phase PbO (lithargyrum) with lower crystallinity in nature, and the resultant $CH_3NH_3PbI_3$ film shows a surface morphology with high uniformity and good coverage over a large area. Also the perovskite film was well crystalized with the grain size of 50–600 nm, exhibiting strong light harvest capability. The solar cells we fabricated employ a NRT contact layer, which is beneficial to extract photogenerated electrons more effectively and prepare the PSCs at low temperature. The champion cells with active area of 0.09 cm^2 and 1.07 cm^2 achieve the best PCE of 14.1% and 10.7%, respectively, under standard AM 1.5 conditions; further enhancement could be expected through following the optimization of the process conditions, adjustment of parameters, etc. The present approach is spin-coating-free for the formation of large area $CH_3NH_3PbI_3$ film with the advantages of easy control, cost-saving, and less use of toxic reagents; more importantly, it is expected to be used for the manufacture of PSCs or other thin-film devices, thus with potential applications and practical significance.

Acknowledgments

This work is supported partially by National High-tech R & D Program of China (863 Program, No. 2015AA034601), National Natural Science Foundation of China (Grant nos. 91333122, 61204064, 51202067, 51372082, 51402106 and 11504107), Ph.D. Programs Foundation of Ministry of Education of China (Grant nos. 20120036120006, 20130036110012), Par-Eu Scholars Program, Fundamental Research Funds for the Central Universities (Grant nos. 2016JQ01, 2015ZZD03, 2015ZD07, 2015XS59), and Program of Educational Department of Gansu Province of China (Grant no. 2016B-096).

Appendix A. Supporting information

Supplementary data associated with this article can be found in the online version at doi:10.1016/j.solmat.2017.01.034.

References

[1] G. Xing, N. Mathews, S. Sun, S.S. Lim, Y.M. Lam, M. Grätzel, et al., Long-range balanced electron-and hole-transport lengths in organic-inorganic $CH_3NH_3PbI_3$, Science, vol. 342(6156), pp. 344–347, ⟨http://dx.doi.org/10.1126/science.1243167⟩.
[2] S.D. Stranks, G.E. Eperon, G. Grancini, C. Menelaou, M.J.P. Alcocer, T. Leijtens, et al., Electron-hole diffusion lengths exceeding 1 μm in an organometal trihalide perovskite absorber, Science 342 (2013) 341–344. http://dx.doi.org/10.1126/science.1243982.
[3] G.E. Eperon, S.D. Stranks, C. Menelaou, M.B. Johnston, L.M. Herz, H.J. Snaith, Formamidinium lead trihalide: a broadly tunable perovskite for efficient planar heterojunction solar cells, Energy Environ. Sci. 7 (2014) 982. http://dx.doi.org/10.1039/c3ee43822h.
[4] T.M. Koh, K. Fu, Y. Fang, S. Chen, T.C. Sum, N. Mathews, Formamidinium-Containing Metal-Halide: An Alternative Material for Near-IR Absorption Perovskite Solar Cells, 2013.
[5] M.M. Lee, J. Teuscher, T. Miyasaka, T.N. Murakami, H.J. Snaith, Efficient hybrid solar cells based on meso-superstructured organometal halide perovskites, Science 338 (2012) 643–647. http://dx.doi.org/10.1126/science.1228604.
[6] W.S. Yang, J.H. Noh, N.J. Jeon, Y.C. Kim, S. Ryu, J. Seo, et al., High-performance photovoltaic perovskite layers fabricated through intramolecular exchange, Science, vol. 348(6240), pp. 1234–1237, ⟨http://dx.doi.org/10.1126/science.aaa9272⟩.
[7] G. Sfyri, C. Vijay, D. Raptis, V. Dracopoulos, P. Lianos, solar energy materials & solar cells study of perovskite solar cells synthesized under ambient conditions and of the performance of small cell modules, Sol. Energy Mater. Sol. Cells 134 (2015) 60–63. http://dx.doi.org/10.1016/j.solmat.2014.11.034.
[8] Z. Zhang, D. Wei, B. Xie, X. Yue, M. Li, ScienceDirect High reproducibility of perovskite solar cells via a complete spin-coating sequential solution deposition process, Sol. Energy 122 (2015) 97–103. http://dx.doi.org/10.1016/j.solener.2015.08.028.
[9] T. Minemoto, M. Murata, Theoretical analysis on effect of band offsets in perovskite solar cells, Sol. Energy Mater. Sol. Cells 133 (2015) 8–14. http://dx.doi.org/10.1016/j.solmat.2014.10.036.
[10] X. Liu, M. Lei, Y. Zhou, B. Song, Y. Li, High performance planar p-i-n perovskite solar cells with crown-ether functionalized fullerene and LiF as double cathode buffer layers, Appl. Phys. Lett. 107 (2015) 063901. http://dx.doi.org/10.1063/1.4928535.
[11] J. Burschka, N. Pellet, S.-J. Moon, R. Humphry-Baker, P. Gao, M.K. Nazeeruddin, et al., Sequential deposition as a route to high-performance perovskite-sensitized solar cells, Nature 499 (2013) 316–319. http://dx.doi.org/10.1038/nature12340.
[12] M. Liu, M.B. Johnston, H.J. Snaith, Efficient planar heterojunction perovskite solar cells by vapour deposition, Nature 501 (2013) 395–398. http://dx.doi.org/10.1038/nature12509.
[13] Q. Chen, H. Zhou, Z. Hong, S. Luo, H.-S. Duan, H.-H. Wang, et al., Planar heterojunction perovskite solar cells via vapor assisted solution process, J. Am. Chem. Soc. (2013) 3–6. http://dx.doi.org/10.1021/ja411509g.
[14] D. Bi, W. Tress, M.I. Dar, P. Gao, J. Luo, C. Renevier, et al., Efficient luminescent solar cells based on tailored mixed-cation perovskites, Sci. Adv. 2 (2016). http://dx.doi.org/10.1126/sciadv.1501170.
[15] M. Grätzel, L. Han, Efficient and Stable Large-area Perovskite Solar Cells with Inorganic Charge Extraction Layers, 2015, pp. 1–10, ⟨http://dx.doi.org/10.1126/science.aad1015⟩.
[16] Z. Yang, B. Cai, B. Zhou, T. Yao, W. Yu, S. (Frank) Liu, et al., An up-scalable approach to CH3NH3PbI3 compact films for high-performance perovskite solar cells, Nano Energy 15 (2015) 670–678. http://dx.doi.org/10.1016/j.nanoen.2015.05.027.
[17] S. Moon, J. Yum, L. Linus, A. Walter, L. Sansonnens, M. Benkhaira, et al., Laser-Scribing Patterning for the Production of Organometallic Halide Perovskite Solar Modules, vol. 5, 2015, pp.1087–1092.
[18] F. Matteocci, S. Razza, F. Di Giacomo, S. Casaluci, G. Mincuzzi, T.M. Brown, et al., Solid-state solar modules based on mesoscopic organometal halide perovskite: a route towards the up-scaling process, Phys. Chem. Chem. Phys. 16 (2014) 3918. http://dx.doi.org/10.1039/c3cp55313b.
[19] A. Fakharuddin, F. Di Giacomo, A.L. Palma, F. Matteocci, I. Ahmed, S. Razza, et al., Vertical tio2 nanorods as a medium for durable and high efficiency perovskite solar modules, ACS Nano (2015) 0–9. http://dx.doi.org/10.1021/acsnano.5b03265.
[20] O. Malinkiewicz, C. Roldán-Carmona, A. Soriano, E. Bandiello, L. Camacho, M.K. Nazeeruddin, et al., Metal-oxide-free methylammonium lead iodide perovskite-based solar cells: the influence of organic charge transport layers, Adv. Energy Mater. (2014) 1–9. http://dx.doi.org/10.1002/aenm.201400345.
[21] M. Yang, Y. Zhou, Y. Zeng, C.S. Jiang, N.P. Padture, K. Zhu, Square-Centimeter solution-processed planar CH3NH3PbI3 perovskite solar cells with efficiency exceeding 15%, Adv. Mater. 27 (2015) 6363–6370. http://dx.doi.org/10.1002/adma.201502586.
[22] S. Razza, F. Di Giacomo, F. Matteocci, L. Cinà, A.L. Palma, S. Casaluci, et al., Perovskite solar cells and large area modules (100 cm2) based on an air flow-assisted PbI2 blade coating deposition process, J. Power Sources 277 (2015) 286–291. http://dx.doi.org/10.1016/j.jpowsour.2014.12.008.
[23] X. Cui, K. Jiang, J.-H. Huang, X. Zhou, M. Su, S. Li, et al., Electrodeposition of PbO and In situ conversion to CH3NH3PbI3 for mesoscopic perovskite solar cells, Chem. Commun. 51 (2015) 1457–1460. http://dx.doi.org/10.1039/c0xx00000x.
[24] J. Huang, K. Jiang, X. Cui, Q. Zhang, M. Gao, M. Su, et al., Direct conversion of CH3NH3PbI3 from electrodeposited PbO for highly efficient planar perovskite solar cells, Sci. Rep. 5 (2015) 15889. http://dx.doi.org/10.1038/srep15889.
[25] A. Yella, L.P. Heiniger, P. Gao, M.K. Nazeeruddin, M. Grätzel, Nanocrystalline rutile electron extraction layer enables low-temperature solution processed perovskite photovoltaics with 13.7% efficiency, Nano Lett. 14 (2014) 2591–2596. http://dx.doi.org/10.1021/nl500399m.
[26] A. Manuscript, Faraday Discussions, 2014, ⟨http://dx.doi.org/10.1039/C4FD00128A⟩.
[27] B. Conings, A. Babayigit, T. Vangerven, J. D'Haen, J. Manca, H.-G. Boyen, The impact of precursor water content on solution-processed organometal halide perovskite films and solar cells, J. Mater. Chem. A 00 (2015) 1–6. http://dx.doi.org/10.1039/C5TA06199G.
[28] J. You, Y. (Michael) Yang, Z. Hong, T.-B. Song, L. Meng, Y. Liu, et al., Moisture assisted perovskite film growth for high performance solar cells, Appl. Phys. Lett. 105 (2014) 183902. http://dx.doi.org/10.1063/1.4901510.
[29] C.-G. Wu, C.-H. Chiang, Z.-L. Tseng, N. Mohammad K, A. Hagfeldt, M. Grätzel, High efficiency stable inverted perovskite solar cells without current hysteresis, Energy Environ. Sci. (2015). http://dx.doi.org/10.1039/C5EE00645G.
[30] S. Venkataraj, J. Geurts, H. Weis, O. Kappertz, W.K. Njoroge, R. Jayavel, et al., Structural and optical properties of thin lead oxide films produced by reactive direct current magnetron sputtering, J. Vac. Sci. Technol. A: Vac. Surf. Films 19 (2001) 2870. http://dx.doi.org/10.1116/1.1410948.
[31] Y. Pauleau, Reactive sputter-deposition and characterization of lead oxide films, J. Vac. Sci. Technol. A: Vac. Surf. Films 14 (1996) 2207. http://dx.doi.org/10.1116/1.580048.
[32] B. Wu, K. Fu, N. Yantara, G. Xing, S. Sun, T.C. Sum, et al., Charge accumulation and hysteresis in perovskite-based solar cells: an electro-optical analysis, Adv. Energy Mater. (2015). http://dx.doi.org/10.1002/aenm.201500829.